BIOCELL

Tech Science Press

http://doi.org/10.32604/biocell.2026.087014

ARTICLE

Depletion of PTGS1 Inhibits IL-1β-Induced Inflammatory Responses and Osteoblast Dysfunction in MC3T3-E1 Cells via the Wnt/β-Catenin Pathway

Danna Cao[1,2], Yiting Lou[1], Li Yang[3], Xuan Yu[4], Binbin Ying[2] and Qianming Chen[1,*]

[1]Stomatology Hospital, School of Stomatology, Zhejiang University School of Medicine, Zhejiang Provincial Clinical Research Center for Oral Diseases, Key Laboratory of Oral Biomedical Research of Zhejiang Province, Cancer Center of Zhejiang University, Engineering Research Center of Oral Biomaterials and Devices of Zhejiang Province, No. 166, Qiutao North Road, Shangcheng District, Hangzhou, China

[2]Department of Stomatology, The First Affiliated Hospital, Ningbo University, No. 59, Liuting Street, Haishu District, Ningbo, China

[3]Department of Stomatology, Guangdong Hospital of Traditional Chinese Medicine, No. 111, Dade Road, Yuexiu District, Guangzhou, China

[4]Department of Stomatology, Qibei Dental Clinic, Ningbo, No. 488-490, Jiangdong North Road, Yinzhou District, Ningbo, China

*Corresponding Author: Qianming Chen. Email: qmchen@zju.edu.cn

Received: 09 June 2026; Accepted: 09 October 2026; Online first: 20 October 2026

ABSTRACT: Objectives: Temporomandibular joint osteoarthritis (TMJ-OA) is a chronic disorder of the mandibular joint characterized by severe symptoms and extensive damage. This study aims to investigate the role of Prostaglandin-Endoperoxide Synthase 1 (PTGS1) in a mouse calvaria-derived pre-osteoblast cell line (MC3T3-E1 cells) under Interleukin-1 beta (IL-1β)-induced inflammatory conditions, using TMJ-OA as the clinical context for this *in vitro* mechanistic investigation. **Methods:** The association between the IL-1β-mediated inflammatory environment and PTGS1 expression was assessed *in vitro*. PTGS1 expression in IL-1β-stimulated MC3T3-E1 cells was determined by Western blot and quantitative real-time polymerase chain reaction (qPCR). Interleukin-6 (IL-6) levels in cell supernatants were quantified by Enzyme-linked immunosorbent assay (ELISA), and cell behaviors were analyzed by ELISA and flow cytometry. The regulatory role of PTGS1 in the IL-1β pathway was further examined through Western blot. **Results:** Both PTGS1 mRNA and protein levels were significantly upregulated in IL-1β-treated MC3T3-E1 cells compared to the control group ($p < 0.01$). Knockdown of PTGS1 markedly reduced IL-1β-induced cell apoptosis, decreased the secretion of IL-6 and tumor necrosis factor-alpha (TNF-α), and inhibited cell migration ($p < 0.01$). Moreover, PTGS1 depletion reversed IL-1β-mediated changes in bone metabolism-related molecules: it restored the IL-1β-induced downregulation of osteoprotegerin (OPG) and suppressed the IL-1β-induced upregulation of receptor activator of nuclear factor kappa-B ligand (RANKL) ($p < 0.01$). Mechanistically, PTGS1 silencing inhibited the activation of the wingless-related integration site/catenin beta 1 (Wnt/β-catenin) pathway, as indicated by reduced expression of β-catenin, c-Myc, and Cyclin D1 ($p < 0.01$). Treatment with SKL2001 counteracted the effects of PTGS1 depletion, restoring IL-1β-induced apoptosis, inflammation, migration, and the abnormal expression of OPG/RANKL and Wnt/β-catenin pathway components ($p < 0.05$). **Conclusion:** PTGS1 knockdown attenuated IL-1β-induced apoptosis, inflammation, and migration in MC3T3-E1 cells, effects that were associated with suppression of the Wnt/β-catenin pathway. These *in vitro* findings suggest that PTGS1 may modulate osteoblastic responses under inflammatory conditions; however, further validation is required before any conclusion regarding TMJ-OA can be drawn.

KEYWORDS: Interleukin-1 beta; temporomandibular joint osteoarthritis; prostaglandin-endoperoxide synthase 1; Wnt/β-catenin

Copyright © 2026 The Authors. Published by Tech Science Press. This work is licensed under a Creative Commons Attribution 4.0 International License, which permits unrestricted use, distribution, and reproduction in any medium, provided the original work is properly cited.

1 Introduction

Temporomandibular joint osteoarthritis (TMJ-OA) is a common chronic progressive joint disease characterized by an imbalance of coordination between TMJ cartilage and subchondral bone under the joint action of abnormal biomechanical and biological factors [1]. TMJ-OA can be induced by a variety of factors, such as genetics, inflammation, metabolic abnormalities, and injury [2]. When the TMJ is subjected to abnormal mechanical loading, secretion of inflammatory factors from synovial tissue is promoted, and the resulting inflammatory microenvironment contributes to TMJ-OA pathogenesis [3]. Inflammatory factors can promote the differentiation of osteoclast precursor cells into mature osteoclasts, leading to the resorption and remodeling of subchondral bone. At the same time, the activity of osteoblasts is inhibited, and the synthesis and secretion by osteoblasts are also affected.

Prostaglandin-endoperoxide synthase 1 (PTGS1), also known as cyclooxygenase 1 (COX1), is the key enzyme in prostaglandin biosynthesis and acts both as a dioxygenase and as a peroxidase [4]. PTGS1 is mainly expressed in the stomach, kidney, and platelets, and its fundamental functions include modulating the resistance of peripheral vasculature, maintenance of renal blood flow, protection of gastric mucosa, and regulation of platelet aggregation [5]. PTGS1 is also believed to play an important role in the pathophysiological processes of inflammation [4], arthritic diseases [6], and cancers [7]. However, the function of PTGS1 in inflammatory osteoblast dysfunction and its potential function in the modulation of inflammation have not been fully elucidated, particularly in the context of TMJ-OA.

Interleukin-1 beta (IL-1β), an important member of the IL-1 family, has attracted much attention due to its important role in inflammation-related diseases [8]. IL-1β has strong pro-inflammatory activity and can induce a variety of pro-inflammatory mediators, such as cytokines and chemokines [9]. Previous studies have shown that IL-1β may have a certain promoting effect on the process of TMJ-OA, further aggravating the related inflammation [10]. This research intends to analyze the effect of IL-1βon PTGS1 expression and function in MC3T3-E1 pre-osteoblasts, as an *in vitro* mechanistic investigation that may inform future studies on inflammatory bone disorders including TMJ-OA.

To dissect the intracellular signaling mechanisms underlying PTGS1 function in inflammatory osteoblasts, we employed mouse calvaria-derived pre-osteoblast cell line (MC3T3-E1 cells), a well-characterized pre-osteoblast cell line derived from mouse calvaria. Although this cell line does not originate from the mandibular condyle, the core signaling cascades governing osteoblast differentiation and inflammatory responses (e.g., wingless-related integration site/catenin beta 1 (Wnt/β-catenin), NF-κB, and MAPK pathways) are highly conserved across skeletal sites. Furthermore, IL-1β is a well-documented pro-inflammatory cytokine elevated in the synovial fluid of TMJ-OA patients, making this classical inflammatory induction model suitable for investigating the molecular crosstalk between inflammation and osteoblast function relevant to TMJ-OA and related conditions.

2 Materials and Methods

2.1 Cell Culture and Treatment

MC3T3-E1 cells (SNL-518, SUNNCELL, Wuhan, China, having been identified by Short Tandem Repeat (STR) and confirmed to be free from mycoplasma contamination), a pre-osteoblastic line derived from mouse calvaria, were cultured in dulbecco's modified eagle medium (DMEM) (KGM12800N, KeyGEN, Nanjing, China) supplemented with 10% fetal bovine serum (A31608, Invitrogen, Carlsbad, CA, USA) and 1% penicillin-streptomycin (KGY0023, KeyGEN, Nanjing, China) at 37°C in a 5% CO_2 humidified incubator. To establish an *in vitro* inflammatory model, cells were seeded at 2×10^5 cells per well in 6-well plates and

allowed to adhere overnight. Recombinant IL-1β (P5898, Beyotime, Shanghai, China) was dissolved in sterile PBS containing 0.1% bovine serum albumin (BSA) as a carrier protein, according to the manufacturer's instructions. Cells were then treated with 3 ng/mL IL-1β for 24 h to induce the inflammatory phenotype. For the solvent control group, cells were treated with an equivalent volume of BSA/PBS vehicle solution (containing 0.1% BSA without IL-1β) for the same duration. The concentration of IL-1β (3 ng/mL) was selected based on previous studies that established inflammatory models in MC3T3-E1 cells using IL-1β at concentrations ranging from 0 to 5 ng/mL [11,12].

2.2 Small Interfering RNA (siRNA) Transfection

After establishing the inflammatory model with IL-1β treatment, PTGS1 knockdown was achieved through siRNA-mediated gene silencing, using three experimental groups: a negative control group transfected with a non-targeting siRNA (si-con, purchased from GenePharma, A01001, Jiangsu, China), and two experimental groups transfected with distinct PTGS1-specific siRNA duplexes (si-PTGS1-1, 5′-GCAGCACTTGAGTGGCTATTT-3′ and si-PTGS1-2, 5′-GTGAGCTACTATACTCGCATT-3′) to ensure target specificity and confirm the observed effects. Cells were seeded to reach 30–50% confluence before transfection. siRNA duplexes were diluted in serum-free medium to the target concentration (50 nM), mixed with Lipofectamine RNAiMAX (13778075, Invitrogen, Waltham, MA, USA, following the manufacturer's instructions), and incubated at room temperature for 5–20 min to form siRNA-lipid complexes. The mixture was added dropwise to cells, followed by gentle agitation for even distribution. After 4–6 h at 37°C, the transfection medium was replaced with fresh complete medium to minimize cytotoxicity. Cells were incubated for an additional 48 h to ensure efficient knockdown. Transfection efficiency was assessed by qPCR (mRNA) and Western blot (protein).

2.3 SKL2001 Treatment

SKL2001 (MCE, HY-101085, New Jersey, USA) was dissolved in DMSO as a stock solution and diluted with culture medium to a final concentration of 10 μM. The final DMSO concentration in the group was maintained at 0.05%, a concentration previously reported to have no significant cytotoxic effects on MC3T3-E1 cells [13]. At 48 h post-siRNA transfection, cells were treated with SKL2001 (10 μM) for 18 h prior to subsequent assays [14].

2.4 Cell Viability Assay

Cell viability was assessed using the cell counting kit-8 (CCK-8, HY-K0301, MCE, Monmouth Junction, NJ, USA) assay. Cells were seeded in 96-well plates at 2×10^3 cells per well and allowed to adhere overnight. Cells were then stimulated with IL-1β for 24 h to establish the inflammatory model. Following IL-1β stimulation, cells were transfected with si-PTGS1 or si-con using Lipofectamine RNAiMAX. At 48 h post-transfection, cells in the rescue group were treated with the Wnt/β-catenin activator SKL2001 (10 μM) for an additional 18 h [14]. At the end of all treatments, the medium was aspirated, and 100 μL of fresh medium containing 10 μL of CCK-8 reagent was added to each well. After incubation at 37°C for 1.5 h, absorbance at 450 nm was measured using a microplate reader (Bio-Rad, iMark, Hercules, CA, USA). All experiments were performed in triplicate.

2.5 Enzyme-Linked Immunosorbent Assay (ELISA)

The cell culture supernatants of MC3T3-E1 cells were collected and centrifuged at 1000× *g* for 10 min at 4°C to remove cellular debris. The concentrations of IL-6 and tumor necrosis factor-alpha (TNF-α)

in the supernatants were determined using mouse-specific ELISA kits (IL-6: PI326, Beyotime, Shanghai, China; TNF-α: PT512, Beyotime, Shanghai, China) strictly according to the manufacturer's protocols. The absorbance of each well was measured at 450 nm using a microplate reader (Bio-Rad, iMark, Hercules, CA, USA). A standard curve was generated for each assay using serially diluted standards provided in the kits. All samples were measured in duplicate to ensure assay reliability.

2.6 qPCR

Total RNA from MC3T3-E1 cells was extracted using TRIzol (CWO581S, CWBIO, Jiangsu, China), and concentration/purity were assessed via a NanoDrop 2000 Spectrophotometer (Thermo Fisher Scientific Inc., Waltham, MA, USA). RNA was reverse-transcribed into cDNA using a reverse transcription kit (CW2569M, CWBIO, Jiangsu, China). Quantitative real-time PCR (qPCR) was performed in a total reaction volume of 20 μL, containing 10 μL of 2× SYBR Green Master Mix (CW0957M, CWBIO, Jiangsu, China), 0.8 μL each of forward and reverse gene-specific primers, 2 μL of cDNA template, and 6.4 μL of nuclease-free water. All reactions were run in triplicate on a CFX96 Touch Real-Time PCR System (Bio-Rad Laboratories, Inc., Hercules, CA, USA). The thermocycling profile was as follows: initial denaturation at 95°C for 10 min, followed by 40 cycles of denaturation at 95°C for 15 s, and annealing/extension at 60°C for 60 s. To verify single-product amplification and exclude non-specific amplicons or primer dimers, a melting curve analysis was performed immediately after the amplification cycles, with a temperature ramp from 65°C to 95°C at 0.5°C increments for 5 s per step. Ct values were normalized to GAPDH, and relative expression was calculated using the $2^{-\Delta\Delta Ct}$ method. The primers were listed below:

PTGS1 (NM_008969.4):
Forward primer: 5′-TTGCACATCCATCCACTCCC-3′,
Reverse primer: 5′-CCTGGTTCTGGCACGGATAG-3′;
OPG (NM_008764.4):
Forward primer: 5′-TCCGGAAACAGAGAAGCCAC-3′,
Reverse primer: 5′-CTTGTGAGCTGTGTCTCCGT-3′;
RANKL (NM_011613.4):
Forward primer: 5′-AGGGAGCACGAAAAACTGGT-3′,
Reverse primer: 5′-CCCCAAAGTACGTCGCATCT-3′;
GAPDH (NM_008084):
Forward primer: 5′-CATCACTGCCACCCAGAAGACTG-3′,
Reverse primer: 5′-ATGCCAGTGAGCTTCCCGTTCAG-3′.

2.7 Western Blot

Cells were lysed in radioimmunoprecipitation assay buffer (CW2333S, CWBIO, Jiangsu, China) containing protease inhibitors (CW2200S, CWBIO, Jiangsu, China), and protein concentration was determined via bicinchoninic acid assay (CW0014S, CWBIO, Jiangsu, China). Equal protein amounts were separated by 10% sodium dodecyl sulfate-polyacrylamide gel electrophoresis and transferred to polyvinylidene difluoride membranes (IPVH00010, Merck, Darmstadt, Germany). Membranes were blocked with 5% non-fat milk, incubated overnight at 4°C with primary antibodies anti-PTGS1 (ab109025, Abcam, Cambridge, UK; 1:1000), anti-OPG (ab183910, Abcam, Cambridge, UK; 1:500), anti-RANKL (ab9957, Abcam, Cambridge, UK; 1:200), anti-c-Myc (ab205818, Abcam, Cambridge, UK; 1:5000), anti-Cyclin D1 (ab190564, Abcam, Cambridge, UK; 1:5000), β-catenin (ab32572, Abcam, Cambridge, UK; 1:5000), Bcl-2 (ab194583, Abcam, Cambridge, UK; 1:1000), Bax (ab182733, Abcam, Cambridge, UK; 1:2000), cleaved Caspase-3 (ab32042, Abcam, Cambridge,

UK; 1:500) and anti-GAPDH (ab181602, Abcam, Cambridge, UK; 1:10,000), then with HRP-conjugated goat anti-rabbit secondary antibody (ab205718, Abcam, Cambridge, UK; 1:5000) for 1 h at room temperature. Bands were visualized via enhanced chemiluminescence (B500024, Proteintech Group, Wuhan, China) and imaged. Specifically, we used ImageJ software (version 1.8.0, National Institutes of Health, Bethesda, MD, USA) to measure the integrated optical density of each band. After subtracting the background, the values were normalized to the internal reference (GAPDH) expressed in the same lane.

2.8 Flow Cytometry

Cell apoptosis was evaluated using an Annexin V-FITC/7-AAD Apoptosis Detection Kit (C1053S, Beyotime, Shanghai, China) according to the manufacturer's instructions. After treatment, cells were harvested, washed with cold PBS (1×, pH 7.4), and resuspended in 1× Annexin V Binding Buffer at a density of 1×10^5 cells/100 μL. A 100 μL aliquot was stained with 5 μL of Annexin V-FITC and 5 μL of 7-AAD, and incubated for 15 min at room temperature in the dark. After adding 400 μL of 1× Binding Buffer, the samples were analyzed within 1 h by flow cytometry (BD Biosciences, San Jose, CA, USA). A total of 10,000 events were acquired per sample. Data were processed using FlowJo software (version 10.8, FlowJo LLC, Ashland, OR, USA) to quantify cell apoptosis.

2.9 Wound Healing Assay

Cell migration was evaluated via a wound healing assay. Cells were seeded to confluence, and a uniform scratch was made using a standard 200 μL pipette tip. After washing with PBS (1×, pH 7.4), cells were incubated with fresh serum-free medium (± treatment) and imaged at 0 h and 24 h post-scratch using phase-contrast microscopy (OLYMPUS, CKX53, Olympus Corporation, Tokyo, Japan). Images were analyzed using ImageJ software (version 1.8.0, National Institutes of Health, Bethesda, MD, USA). The wound width was measured at five random fields per well using the straight-line tool. The wound closure rate was calculated as: $(W_0 - W_{24})/W_0 \times 100\%$, where W_0 and W_{24} represent the wound width at 0 h and 24 h, respectively.

2.10 Transwell Assay

Cell migration in response to chemoattractants was assessed using Transwell inserts (8 μm MCEP24H48, Merck, Darmstadt, Germany). Cells were resuspended in serum-free medium and seeded into the upper chamber at a density of 5×10^4 cells per well in 100 μL of serum-free medium. The lower chamber was filled with 600 μL of medium containing 10% fetal bovine serum (FBS) to establish a chemotactic gradient. After 24 h, non-migrated cells were removed with a cotton swab, and migrated cells were fixed with 4% paraformaldehyde, stained with 0.1% crystal violet for 15 min at room temperature, imaged (OLYMPUS, CKX53, Olympus Corporation, Tokyo, Japan), and counted across five fields.

2.11 Statistical Analysis

Data were presented as mean ± standard deviation (SD). All experiments were performed in triplicate. Normality of the data was assessed using the Shapiro–Wilk test. Homogeneity of variance was verified using Levene's test. For comparisons between two groups, a Student's *t*-test was used. For comparisons among multiple groups, one-way or two-way analysis of variance (ANOVA) followed by Tukey's *post hoc* tests was applied. For data that did not meet the assumptions of normality or equal variance, the non-parametric Kruskal–Wallis test (for multiple groups) or Mann–Whitney U test (for two groups) was used instead. A

p-value < 0.05 was considered statistically significant. GraphPad Prism software 8.0 (GraphPad Software, San Diego, CA, USA) was used for statistical analysis and graph generation.

3 Results

3.1 The Inflammation Model of MC3T3-E1 Cells Induced by IL-1β Was Established

After MC3T3-E1 cells were treated with IL-1β, the CCK-8 assay and ELISA were used to detect changes in cell activity and IL-6 expression levels in the cell supernatant. CCK-8 assay was used to detect differences in cell viability in the control group, BSA group (solvent group), and IL-1β group, as shown in Fig. 1A. At 24 h, there was no significant difference in cell viability between the BSA-treated and IL-1β-treated MC3T3-E1 cells, indicating that IL-1β did not cause an obvious reduction in cell viability at this time point. After confirming that 24 h IL-1β treatment did not markedly reduce MC3T3-E1 cells viability, ELISA was used to detect the expression level of IL-6 in the supernatant of IL-1β-treated cells, as shown in Fig. 1B. Compared with the control group, the expression level of IL-6 in the cell supernatant was significantly increased after 24 h stimulation with IL-1β, suggesting that the model was successfully induced.

3.2 IL-1β Activated the Expression of PTGS1 in MC3T3-E1 Cells

Afterward, the mRNA and protein levels of PTGS1 were examined by qPCR and Western blot assays. As shown in Fig. 1C–E, the mRNA of PTGS1 was significantly upregulated in the IL-1β-activated cells, and Western blot results showed that IL-1β treatment effectively stimulated the protein expression of PTGS1, suggesting that IL-1β effectively activated the expression of PTGS1.

3.3 Silencing PTGS1 Inhibited Apoptosis, Inflammation, and Migration in IL-1β-Induced MC3T3-E1 Cells

To further detect the function of PTGS1 in IL-1β-induced MC3T3-E1 cells, si-PTGS1 was applied. As shown in Fig. 1F–H, the mRNA and protein expression of PTGS1 were significantly decreased after si-PTGS1-1 or si-PTGS1-2 treatment. Then, flow cytometry, ELISA, Transwell, and wound healing assays were performed to detect apoptosis, inflammation, and migration of MC3T3-E1 cells. Compared with the control group, IL-1β induced an increase in apoptosis of MC3T3-E1 cells, while silencing PTGS1 inhibited IL-1β-induced apoptosis of MC3T3-E1 cells (Fig. 2A). Consistently, Western blot analysis showed that IL-1β decreased Bcl-2 expression and increased Bax and cleaved caspase-3 expression, whereas PTGS1 silencing reversed these changes, in agreement with the flow cytometry results (Fig. 2B,C). As shown in Fig. 2D,E, the expression of IL-6 and TNF-α was activated by IL-1β, which was suppressed by PTGS1 knockdown. In the advanced stage of TMJ-OA, the condyle exhibits typical pathological features including osteophyte formation and subchondral bone sclerosis/remodeling [15]. These changes are attributed to complex pathophysiological processes, in which the migratory ability of osteoblasts plays a key role in the aberrant subchondral bone turnover [16]. Compared with the control group, the number of cell migrations increased in the IL-1β group, but PTGS1 knockdown reduced the increase in the number of cell migrations induced by IL-1β (Fig. 3A). Similarly, the wound closure rate was increased in the IL-1β group compared with the control group, whereas PTGS1 depletion diminished the wound closure rate of MC3T3-E1 cells (Fig. 3B).

3.4 Knockdown of PTGS1 Altered the Expression of OPG and RANKL, and Suppressed the Wnt/β-Catenin Pathway

It is well known that OPG is a protective factor for bones, helping to maintain bone density and strength, and RANKL contributes to bone resorption and remodeling [17]. In this study, we discovered

that the expression of OPG was decreased in the IL-1β group, and knockdown of PTGS1 inhibited the IL-1β-induced decrease in OPG expression (Fig. 4A–C). Moreover, RANKL expression was increased in the IL-1β group, and knockdown of PTGS1 diminished the IL-1β-induced increase in RANKL expression (Fig. 4D–F). Additionally, the expression levels of c-Myc, Cyclin D1 and β-catenin were increased in the IL-1β group, whereas knockdown of PTGS1 inhibited the increase in IL-1β-induced expression of c-Myc, Cyclin D1 and β-catenin (Fig. 4G,H).

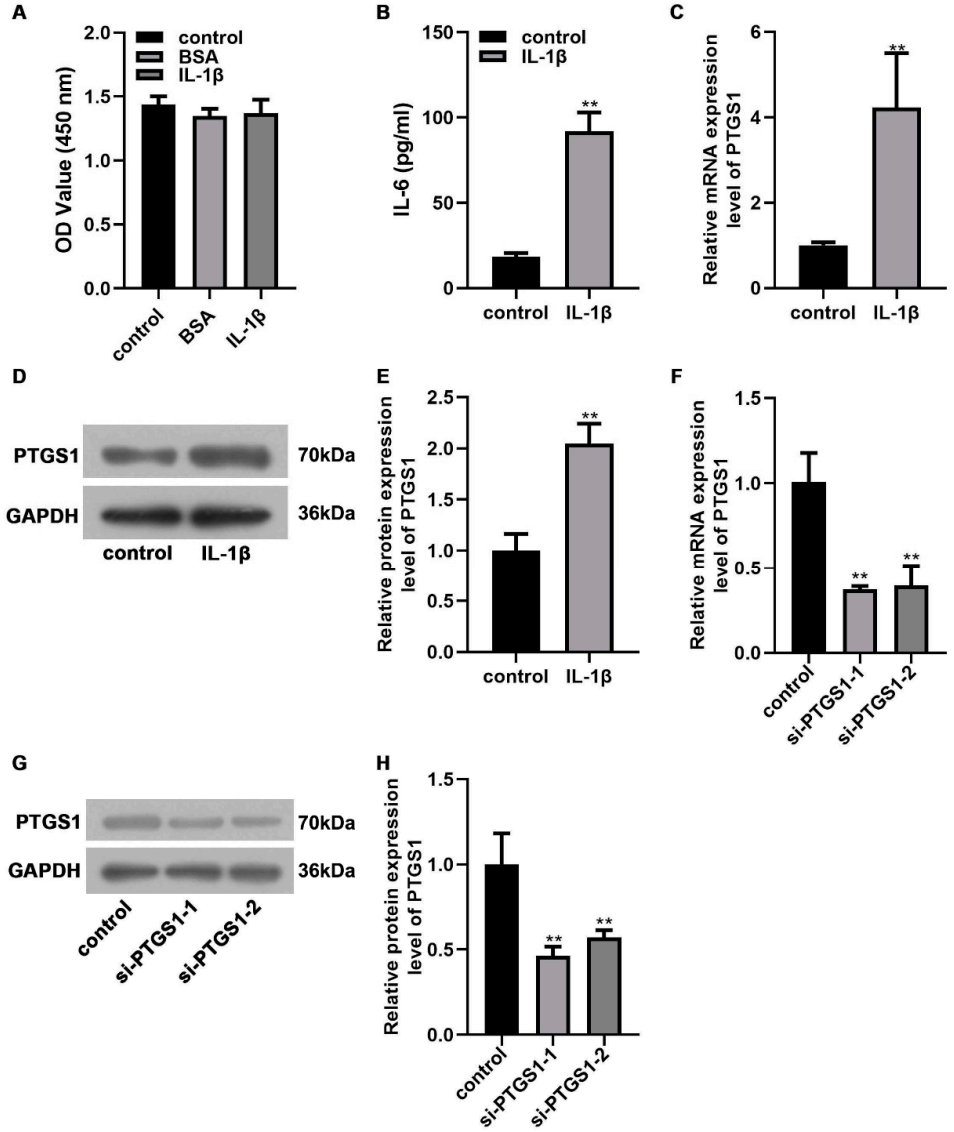

Figure 1: IL-1β was used to stimulate MC3T3-E1 cells to mimic the inflammation models *in vitro*. (**A**). CCK-8 assay was used to detect the viability of MC3T3-E1 cells after IL-1β treatment. (**B**). ELISA was used to detect IL-6 expression in IL-1β-induced MC3T3-E1 cells. (**C**–**E**). qPCR and Western blot assays were used to detect PTGS1 expression in IL-1β-induced MC3T3-E1 cells. (**F**–**H**). qPCR and Western blot assays were used to detect PTGS1 expression after si-PTGS1-1 or si-PTGS1-2 treatment. $^{**}p < 0.01$ vs. control. Data are presented as mean ± SD, n = 3 independent experiments; *p* values were calculated using Student's *t*-test for two-group comparisons and one-way ANOVA followed by Tukey's *post-hoc* test for multiple-group comparisons.

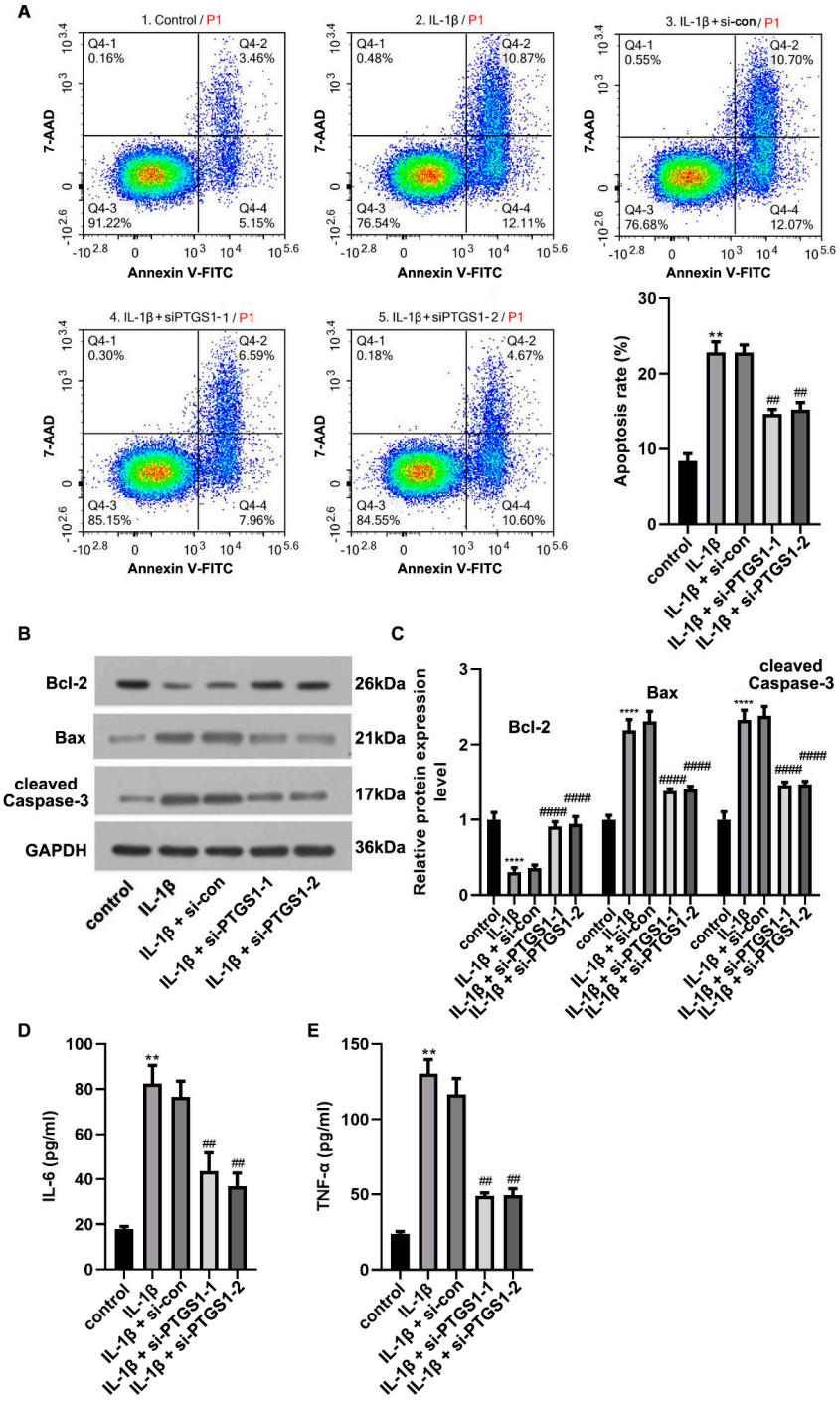

Figure 2: Silencing PTGS1 inhibited the apoptosis and inflammation of MC3T3-E1 cells induced by IL-1β. (**A**). Flow cytometry was used to detect the apoptosis rate of IL-1β-induced MC3T3-E1 cells after si-PTGS1-1 or si-PTGS1-2 treatment. (**B**,**C**). Western blot assays were used to detect Bcl-2, Bax, and cleaved Caspase-3 expression in IL-1β-induced MC3T3-E1 cells after si-PTGS1-1 or si-PTGS1-2 treatment. (**D**,**E**). ELISA was used to detect IL-6 and TNF-α expression in IL-1β-induced MC3T3-E1 cells after si-PTGS1-1 or si-PTGS1-2 treatment. $^{**}p < 0.01$, $^{****}p < 0.0001$ vs. control, $\#\#p < 0.01$, $\#\#\#\#p < 0.0001$ vs. IL-1β + si-con. Data are presented as mean ± SD, n = 3 independent experiments; *p* values were calculated using Student's *t*-test for two-group comparisons and one-way ANOVA followed by Tukey's *post-hoc* test for multiple-group comparisons.

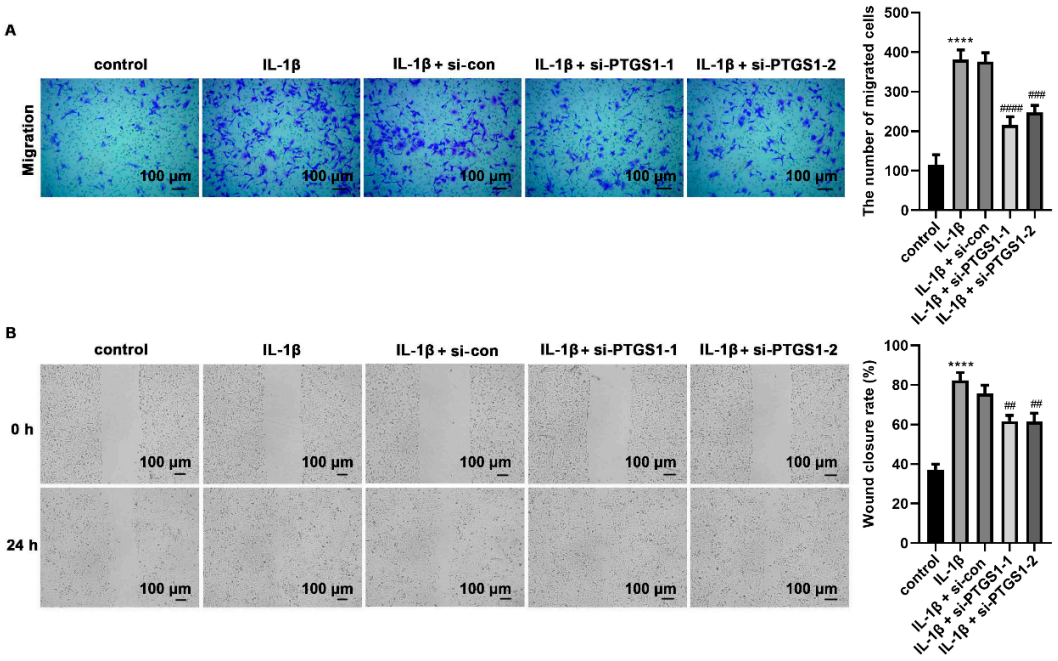

Figure 3: Depletion of PTGS1 suppressed the migratory ability of IL-1β-induced MC3T3-E1 cells. (**A**). A Transwell assay was used to detect the migratory ability of IL-1β-induced MC3T3-E1 cells after si-PTGS1-1 or si-PTGS1-2 treatment. (**B**). Wound healing assay was used to detect the wound closure rate of IL-1β-induced MC3T3-E1 cells after si-PTGS1-1 or si-PTGS1-2 treatment. $^{****}p < 0.0001$ vs. control, $\#\#p < 0.01$, $\#\#\#p < 0.001$, $\#\#\#\#p < 0.0001$ vs. IL-1β + si-con. Data are presented as mean ± SD, n = 3 independent experiments; *p* values were calculated using Student's *t*-test for two-group comparisons and one-way ANOVA followed by Tukey's *post-hoc* test for multiple-group comparisons.

3.5 Activation of the Wnt/β-Catenin Pathway Could Reverse the Function of PTGS1 Knockdown in IL-1β-Induced MC3T3-E1 Cells

To further detect the relationship between PTGS1 and the Wnt/β-catenin pathway, SKL2001 (Wnt/β-catenin agonist) was applied. SKL2001 treatment could diminish the inhibitory effects of si-PTGS1 on the apoptosis, IL-6 and TNF-α expression, and wound closure rate in IL-1β-induced MC3T3-E1 cells (Fig. 5). Moreover, the SKL2001 treatment could reverse the promoting effect of si-PTGS1 on OPG expression and the suppressive effect of si-PTGS1 on RANKL expression in IL-1β-induced MC3T3-E1 cells (Fig. 6). Therefore, our findings demonstrated that si-PTGS1 performed beneficial effects by inactivating Wnt/β-catenin pathway in IL-1β-induced MC3T3-E1 cells.

4 Discussion

In this study, we investigated the role of PTGS1 in IL-1β-induced MC3T3-E1 cells and established that PTGS1 modulates IL-1β-induced phenotypic changes in MC3T3-E1 pre-osteoblasts. Our findings demonstrated that PTGS1 was significantly upregulated in IL-1β-induced MC3T3-E1 cells and played a critical role in regulating cellular apoptosis, inflammation, and migration. Depletion of PTGS1 significantly attenuated IL-1β-induced apoptosis, inflammatory responses, and migratory capabilities in MC3T3-E1 cells. Furthermore, we observed that PTGS1 depletion reversed the IL-1β-induced decrease in OPG expression and the increase in RANKL expression, suggesting a potential regulatory role of PTGS1 in bone remodeling and osteoblastogenesis. Mechanistically, PTGS1 depletion suppresses the Wnt/β-catenin pathway, and

the subsequent rescue with SKL2001 confirms that this pathway mediates the protective effects of PTGS1 silencing. Collectively, these data indicate that PTGS1 modulates IL-1β-induced cellular responses and is functionally associated with the Wnt/β-catenin pathway in MC3T3-E1 cells.

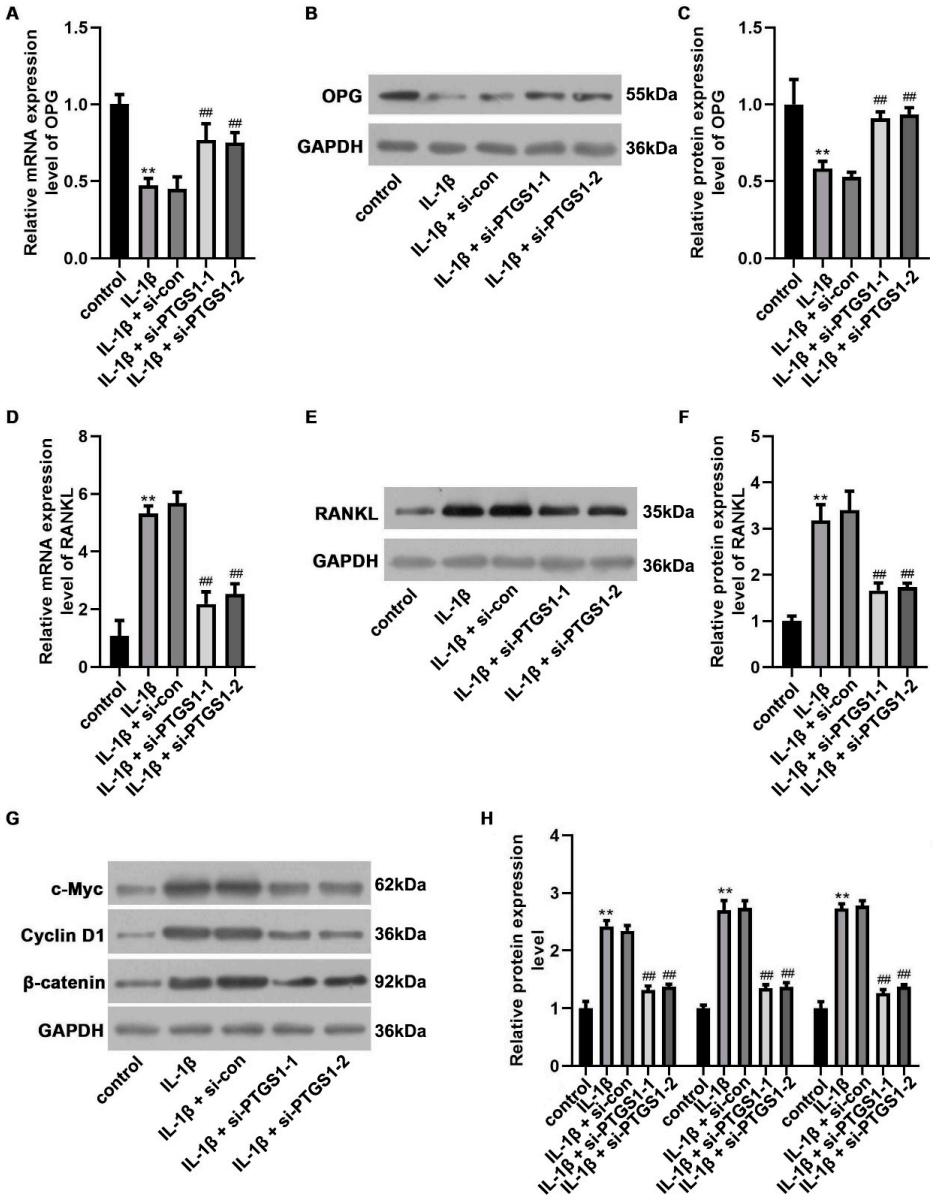

Figure 4: Knockdown of PTGS1 altered the expression of OPG and RANKL, and suppressed the Wnt/β-catenin pathway. (**A**–**F**). Expression levels of OPG and RANKL were measured by qPCR and Western blot assay in IL-1β-induced MC3T3-E1 cells after si-PTGS1-1 or si-PTGS1-2 treatment. (**G**,**H**). Expression levels of c-Myc, Cyclin D1, and β-catenin were measured by Western blot assay in IL-1β-induced MC3T3-E1 cells after si-PTGS1-1 or si-PTGS1-2 treatment. $^{**}p < 0.01$ vs. control, $\#\#p < 0.01$ vs. IL-1β + si-con. Data are presented as mean ± SD, n = 3 independent experiments; *p* values were calculated using Student's *t*-test for two-group comparisons and one-way ANOVA followed by Tukey's *post-hoc* test for multiple-group comparisons.

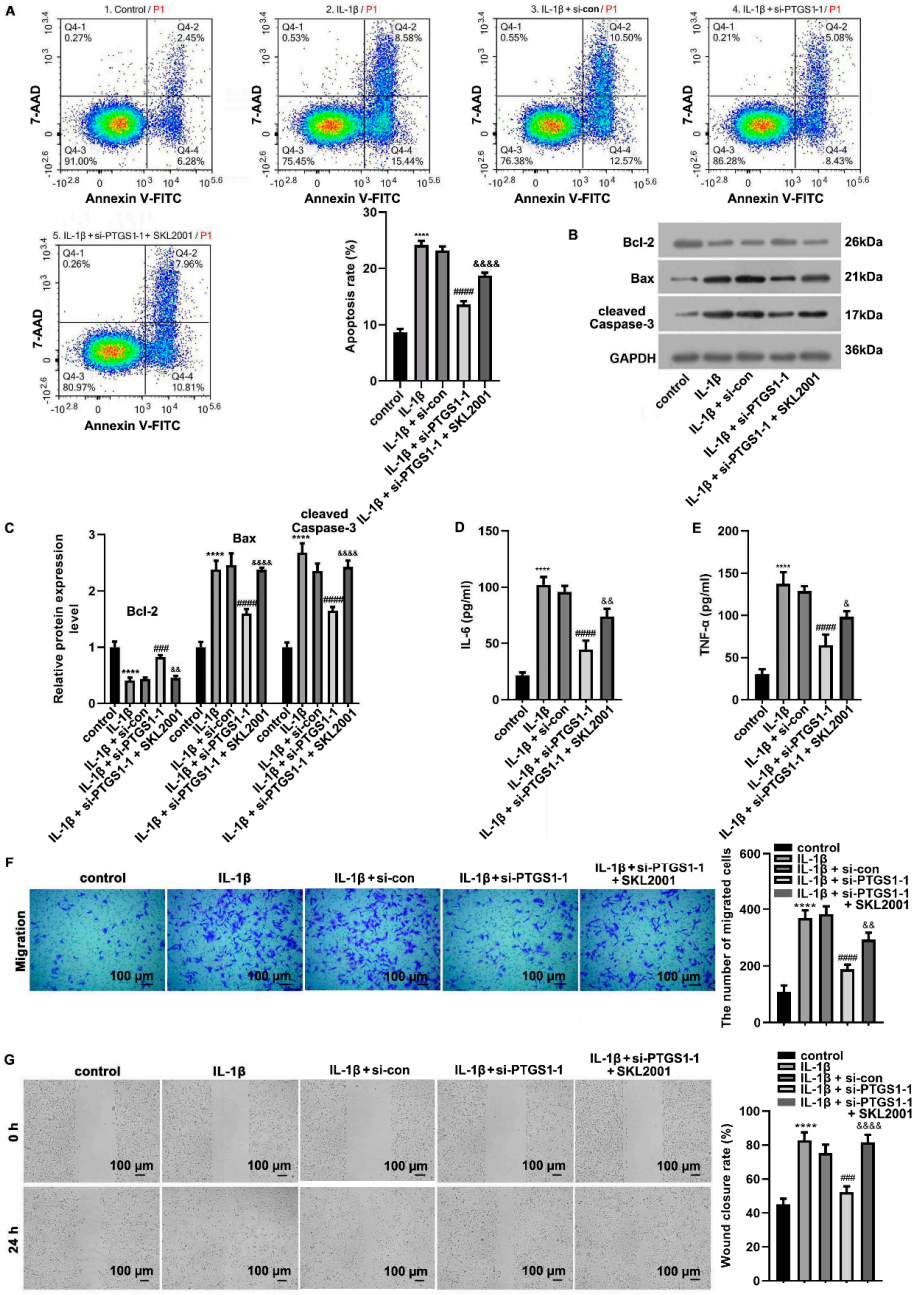

Figure 5: Activation of the Wnt/β-catenin pathway could reverse the function of PTGS1 knockdown in IL-1β-induced MC3T3-E1 cells. (**A**). Apoptosis was measured by a flow cytometry assay in IL-1β-induced MC3T3-E1 cells after si-PTGS1-1 and si-PTGS1-1 + SKL2001 treatment. (**B**,**C**). Western blot assays were used to detect Bcl-2, Bax, and cleaved Caspase-3 expression in IL-1β-induced MC3T3-E1 cells after si-PTGS1-1 and si-PTGS1-1 + SKL2001 treatment. (**D**,**E**). Levels of IL-6 and TNF-α were measured by ELISA in IL-1β-induced MC3T3-E1 cells after si-PTGS1-1 and si-PTGS1-1 + SKL2001 treatment. (**F**,**G**). The migratory ability was measured by transwell and wound healing assays in IL-1β-induced MC3T3-E1 cells after si-PTGS1-1 and si-PTGS1-1 + SKL2001 treatment. ****$p < 0.0001$ vs. control; ###$p < 0.001$, ####$p < 0.0001$ vs. IL-1β + si-con; &$p < 0.05$, &&$p < 0.01$, &&&&$p < 0.0001$ vs. IL-1β + si-PTGS1-1. Data are presented as mean ± SD, n = 3 independent experiments; p values were calculated using Student's *t*-test for two-group comparisons and one-way ANOVA followed by Tukey's *post-hoc* test for multiple-group comparisons.

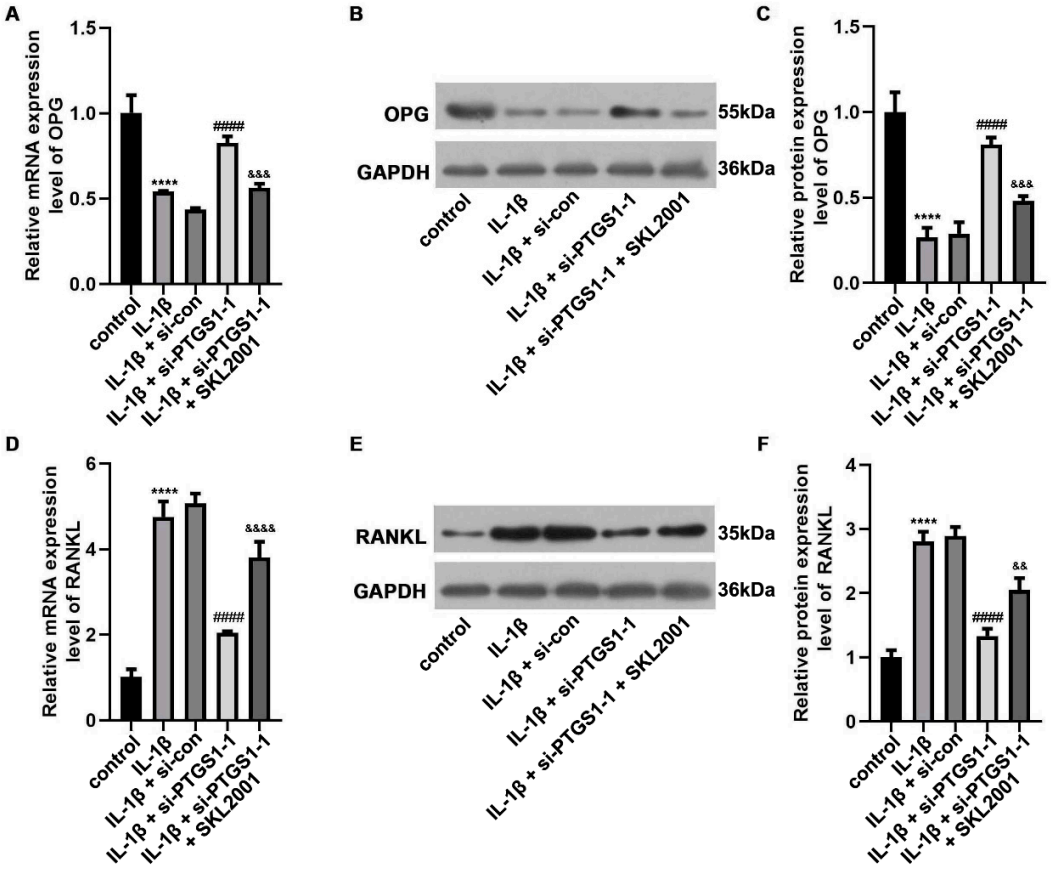

Figure 6: SKL2001 treatment could reverse the promoting effect of si-PTGS1-1 on OPG expression and RANKL inhibition in IL-1β-induced MC3T3-E1 cells. (**A**–**F**). Expression levels of OPG and RANKL were measured by qPCR and Western blot assay in IL-1β-induced MC3T3-E1 cells after si-PTGS1-1 and si-PTGS1-1 + SKL2001 treatment. $^{****}p < 0.0001$ vs. control, $\#\#\#\#p < 0.0001$ vs. IL-1β + si-con, $\&\&p < 0.01$, $\&\&\&p < 0.001$, $\&\&\&\&p < 0.0001$ vs. IL-1β + si-PTGS1-1. Data are presented as mean ± SD, n = 3 independent experiments; *p* values were calculated using Student's *t*-test for two-group comparisons and one-way ANOVA followed by Tukey's *post-hoc* test for multiple-group comparisons.

PTGS1, also known as cyclooxygenase-1 (COX-1), is a key enzyme involved in the biosynthesis of prostaglandins and thromboxanes from arachidonic acid [18]. It is constitutively expressed in most tissues and plays a crucial role in maintaining physiological functions, such as gastric mucosal protection, platelet aggregation, and renal homeostasis [19]. Unlike its inducible counterpart, PTGS2 (COX-2), which is primarily associated with inflammation and pain, PTGS1 is generally considered a housekeeping enzyme. However, emerging evidence suggests that PTGS1 may also contribute to pathological processes, including inflammation, cancer, and bone-related diseases [20–22]. Our findings suggest that PTGS1 acts as an important amplifier or mediator of the inflammatory response in osteoblasts, rather than a simple passive marker. Its upregulation by IL-1β and its subsequent impact on downstream inflammatory and bone remodeling pathways place it as a potential intermediate link in the disease cascade. Additionally, the traditionally emphasized role of COX-2 in inflammation and arthritis is well established, whereas COX-1 is often overlooked. Our study highlights the potential significance of COX-1 in inflammatory osteoblast biology, suggesting that both isoforms merit consideration as therapeutic targets in inflammatory bone disorders, including TMJ-OA.

Recent studies have highlighted the role of PTGS1 in inflammatory conditions such as osteoarthritis (OA), where its expression is up-regulated in affected tissues [23]. In the context of bone metabolism, PTGS1 has been implicated in regulating osteoblast activity, influencing bone remodeling processes [24]. We also explored the interplay between PTGS1 and signaling pathways such as Wnt/β-catenin, which are critical for bone formation and resorption. One of the key findings of this study was the involvement of the Wnt/β-catenin signaling pathway in the PTGS1-mediated effects. We found that PTGS1 depletion inhibited the activation of the Wnt/β-catenin pathway, which is known to play a pivotal role in bone metabolism and inflammation. To further validate the role of this pathway, SKL2001 was applied. The results showed that activation of Wnt/β-catenin signaling suppressed the effects of PTGS1 knockdown, further supporting the notion that PTGS1 exerts its effects, at least in part, through the modulation of Wnt/β-catenin signaling. While our data demonstrate a robust functional association, the precise molecular mechanism by which PTGS1 regulates Wnt/β-catenin signaling requires further investigation. It is plausible that PTGS1-derived prostaglandins, such as PGE2, could indirectly modulate the pathway through G protein-coupled receptors (e.g., EP receptors) that crosstalk with Wnt signaling [25]. This represents a critical area for future research to establish whether PTGS1 acts as a direct or indirect regulator of the pathway.

The interplay between PTGS1 and Wnt/β-catenin signaling in TMJ-OA is particularly intriguing. The observed changes in OPG and RANKL expression following PTGS1 knockdown suggest that PTGS1 modulates the secretory profile of osteoblasts under inflammatory conditions. Inflammatory cytokines such as IL-1β are known to increase RANKL expression and decrease OPG expression on osteoblasts [26,27]. By suppressing Wnt/β-catenin signaling, PTGS1 knockdown led to increased OPG and decreased RANKL expression, which may reflect a shift toward a more osteoblast-protective microenvironment [28]. However, alterations in the OPG/RANKL ratio alone do not directly measure osteoblast differentiation or bone-forming capacity. Therefore, future studies should investigate additional markers of osteoblast function, such as osteocalcin (OCN) and alkaline phosphatase (ALP), to provide a more comprehensive assessment of the effects of PTGS1 on osteoblast biology. Wnt/β-catenin signaling has been implicated in both bone formation and resorption, and its dysregulation is often associated with inflammatory bone diseases, including osteoarthritis [29]. Our data suggested that PTGS1 may act as an upstream regulator of this pathway, influencing the balance between bone formation and resorption in TMJ-OA. The observed changes in OPG and RANKL expression following PTGS1 knockdown further supported this hypothesis, as these molecules are critical regulators of osteoblast differentiation and activity.

It is worth noting that Wnt/β-catenin signaling exerts context-dependent effects in the temporomandibular joint. Under physiological conditions, this pathway is essential for chondrocyte survival, matrix homeostasis, and subchondral bone remodeling [25]. However, its sustained or aberrant activation has been implicated in cartilage degradation, osteophyte formation, and synovial inflammation, which are hallmark features of TMJ-OA and other degenerative joint diseases [30]. In the present study, we observed that PTGS1 depletion inhibited the IL-1β-induced upregulation of β-catenin, c-Myc, and Cyclin D1, suggesting that under inflammatory conditions, Wnt/β-catenin signaling shifts toward a pathological role [31]. These findings are consistent with previous reports that the net outcome of Wnt/β-catenin activation depends on the duration, intensity, and cellular context of the signal [32]. Thus, therapeutic strategies for inflammatory joint diseases such as TMJ-OA should consider not merely inhibiting but fine-tuning this pathway to avoid disrupting its beneficial homeostatic functions.

5 Limitations

Despite these insights, our study has limitations. First, it lacks *in vivo* animal experiments, relying solely on an *in vitro* single-cell model, which fails to replicate the complex TMJ microenvironment and validate findings' relevance to actual TMJ-OA pathology. Second, indicator detection is insufficient: it omits bone metabolism (e.g., OCN) and Wnt/β-catenin pathway upstream components (e.g., Wnt ligands, GSK-3β), hindering a comprehensive understanding of PTGS1's regulatory mechanisms in TMJ-OA. Moreover, assessment of the pathway was restricted to total β-catenin, c-Myc, and Cyclin D1, without evaluating β-catenin nuclear translocation, p-GSK3β, or active β-catenin. These aspects should be addressed in future studies.

6 Conclusion

In conclusion, this study demonstrates that PTGS1 knockdown attenuates IL-1β-induced apoptosis, inflammation, and migration in MC3T3-E1 pre-osteoblasts, and reverses IL-1β-induced changes in OPG and RANKL expression. These findings suggest that PTGS1 may represent a potential target for intervention in inflammatory bone disorders. However, given the inherent limitations of the *in vitro* model and the non-TMJ origin of the cell line used, further validation in TMJ-specific experimental systems is required before conclusions can be drawn regarding TMJ-OA pathogenesis. Such future investigations, including *in vivo* studies and exploration of PTGS1 inhibitors, represent essential next steps toward translating these mechanistic insights into therapeutic strategies for TMJ-OA and related conditions.

Acknowledgement: Not applicable.

Funding Statement: This study was supported by Zhejiang Medical and Health Project (2022KY1096) and City youth technical backbone personnel training special (QNJSGG-3-CDN).

Author Contributions: Study conception and design: Danna Cao, Yiting Lou, Qianming Chen; data collection: Danna Cao, Yiting Lou; analysis and interpretation of results: Danna Cao, Yiting Lou, Li Yang, Xuan Yu, Binbin Ying; draft manuscript preparation: Danna Cao, Yiting Lou, Li Yang, Xuan Yu, Binbin Ying, Qianming Chen. All authors reviewed and approved the final version of the manuscript.

Availability of Data and Materials: The datasets used and/or analyzed during the current study are available from the corresponding author on reasonable request.

Ethics Approval: Not applicable.

Conflicts of Interest: All authors declare that there is no conflict of interest in this study.

References

1. Liu X, Li H, Feng Y, Guo H, Li Y, Ke J, et al. Resatorvid alleviates experimental inflammatory TMJOA by restraining chondrocyte pyroptosis and synovial inflammation. Arthritis Res Ther. 2023;25(1):230. [CrossRef].
2. Jiang C, Luo P, Li X, Liu P, Li Y, Xu J. Nrf2/ARE is a key pathway for curcumin-mediated protection of TMJ chondrocytes from oxidative stress and inflammation. Cell Stress Chaperones. 2020;25(3):395–406. [CrossRef].
3. Xue XT, Zhang T, Cui SJ, He DQ, Wang XD, Yang RL, et al. Sexual dimorphism of estrogen-sensitized synoviocytes contributes to gender difference in temporomandibular joint osteoarthritis. Oral Dis. 2018;24(8):1503–13. [CrossRef].
4. Smith WL, DeWitt DL, Garavito RM. Cyclooxygenases: Structural, cellular, and molecular biology. Annu Rev Biochem. 2000;69:145–82. [CrossRef].

5. Faki Y, Er A. Different chemical structures and physiological/pathological roles of cyclooxygenases. Rambam Maimonides Med J. 2021;12(1):e0003. [CrossRef].
6. Farzeen I, Sultana S, Inam S, Ashraf A. Multi-target modulation of inflammatory pathways by *Colchicum luteum* in rheumatoid arthritis through experimental and in silico evidence. Inflammopharmacology. 2026;34(5):3387–412. [CrossRef].
7. Nagao M, Sato Y, Yamauchi A. A meta-analysis of PTGS1 and PTGS2 polymorphisms and NSAID intake on the risk of developing cancer. PLoS One. 2013;8(8):e71126. [CrossRef].
8. Han JH. Immuno-metabolic diseases and therapeutics: Molecular mechanisms *via* inflammasome signaling. Cell Commun Signal. 2025;23(1):373. [CrossRef].
9. Crowson CS, Hein MS, Pendegraft RS, Strausbauch MA, Niewold TB, Ernste FC, et al. Interferon chemokine score and other cytokine measures track with changes in disease activity in patients with juvenile and adult dermatomyositis. ACR Open Rheumatol. 2019;1(2):83–9. [CrossRef].
10. Chen H, Wu G, Sun Q, Dong Y, Zhao H. Hyperbaric oxygen protects mandibular condylar chondrocytes from interleukin-1β-induced apoptosis *via* the PI3K/AKT signaling pathway. Am J Transl Res. 2016;8(11):5108–17.
11. Patil C, Zhu X, Rossa C Jr, Kim YJ, Kirkwood KL. p38 MAPK regulates IL-1beta induced IL-6 expression through mRNA stability in osteoblasts. Immunol Investig. 2004;33(2):213–33. [CrossRef].
12. Murakami M, Kuwata H, Amakasu Y, Shimbara S, Nakatani Y, Atsumi GI, et al. Prostaglandin e2 Amplifies Cytosolic Phospholipase a2- and Cyclooxygenase-2-dependent Delayed Prostaglandin e2 Generation in Mouse Osteoblastic Cells enhancement by secretory phospholipase a2. J Biol Chem. 1997;272(32):19891–7. [CrossRef].
13. Toor RH, Malik S, Qamar H, Batool F, Tariq M, Nasir Z, et al. Osteogenic potential of hexane and dichloromethane fraction of *Cissus quadrangularis* on murine preosteoblast cell line MC3T3-E1 (subclone 4). J Cell Physiol. 2019;234(12):23082–96. [CrossRef].
14. Frey JL, Kim SP, Li Z, Wolfgang MJ, Riddle RC. β-catenin directs long-chain fatty acid catabolism in the osteoblasts of male mice. Endocrinology. 2018;159(1):272–84. [CrossRef].
15. Song HJ, Choi HM, Shin BM, Kim YJ, Park MS, Kim C. Age-stratified analysis of temporomandibular joint osteoarthritis using cone-beam computed tomography. Imaging Sci Dent. 2024;54(1):71–80. [CrossRef].
16. Liu Y, Jia F, Li K, Liang C, Lin X, Geng W, et al. Critical signaling molecules in the temporomandibular joint osteoarthritis under different magnitudes of mechanical stimulation. Front Pharmacol. 2024;15:1419494. [CrossRef].
17. Kanji S, Sarkar R, Pramanik A, Kshirsagar S, Greene CJ, Das H. Dental pulp–derived stem cells inhibit osteoclast differentiation by secreting osteoprotegerin and deactivating AKT signalling in myeloid cells. J Cell Mol Med. 2021;25(5):2390–403. [CrossRef].
18. Dearth CL, Slivka PF, Stewart SA, Keane TJ, Tay JK, Londono R, et al. Inhibition of COX1/2 alters the host response and reduces ECM scaffold mediated constructive tissue remodeling in a rodent model of skeletal muscle injury. Acta Biomater. 2016;31:50–60. [CrossRef].
19. Palma-Barqueros V, Crescente M, de la Morena ME, Chan MV, Almarza E, Revilla N, et al. A novel genetic variant in *PTGS1* affects N-glycosylation of cyclooxygenase-1 causing a dominant-negative effect on platelet function and bleeding diathesis. Am J Hematol. 2021;96(3):E83–8. [CrossRef].
20. Mederle K, Meurer M, Castrop H, Höcherl K. Inhibition of COX-1 attenuates the formation of thromboxane A2 and ameliorates the acute decrease in glomerular filtration rate in endotoxemic mice. Am J Physiol Renal Physiol. 2015;309(4):F332–40. [CrossRef].
21. Park S, Zhu J, Altan-Bonnet G, Cheng SY. Monocyte recruitment and activated inflammation are associated with thyroid carcinogenesis in a mouse model. Am J Cancer Res. 2019;9(7):1439–53.
22. Cortes A, Maksymowych WP, Wordsworth BP, Inman RD, Danoy P, Rahman P, et al. Association study of genes related to bone formation and resorption and the extent of radiographic change in ankylosing spondylitis. Ann Rheum Dis. 2015;74(7):1387–93. [CrossRef].
23. Zhang X, Bu Y, Zhu B, Zhao Q, Lv Z, Li B, et al. Global transcriptome analysis to identify critical genes involved in the pathology of osteoarthritis. Bone Joint Res. 2018;7(4):298–307. [CrossRef].
24. Wang J, Huang Y, Guo L, Li J, Zhou S. Molecular mechanism of Achyranthis bidentatae *Radix* and Morindae officinalis *Radix* in osteoporosis therapy: An investigation based on network pharmacology, molecular docking, and molecular dynamics simulations. Biochem Biophys Rep. 2023;36:101586. [CrossRef].

25. Wang J, Sun L, Zhang Y, Chen S, He Y. Wnt/β-catenin regulates Gli1 + osteogenic progenitors in condylar subchondral bone development and osteoarthritis. BMC Musculoskelet Disord. 2025;26(1):533. [CrossRef].
26. Nakashima T, Kobayashi Y, Yamasaki S, Kawakami A, Eguchi K, Sasaki H, et al. Protein expression and functional difference of membrane-bound and soluble receptor activator of NF-kappaB ligand: Modulation of the expression by osteotropic factors and cytokines. Biochem Biophys Res Commun. 2000;275(3):768–75. [CrossRef].
27. Chatmahamongkol C, Pravitharangul A, Suttapreyasri S, Leethanakul C. The effect of compressive force combined with mechanical vibration on human alveolar bone osteoblasts. J Oral Biol Craniofac Res. 2019;9(1):81–5. [CrossRef].
28. Hu L, Chen W, Qian A, Li YP. Wnt/β-catenin signaling components and mechanisms in bone formation, homeostasis, and disease. Bone Res. 2024;12(1):39. [CrossRef].
29. Haxaire C, Haÿ E, Geoffroy V. Runx2 controls bone resorption through the down-regulation of the Wnt pathway in osteoblasts. Am J Pathol. 2016;186(6):1598–609. [CrossRef].
30. Lu K, Ma F, Yi D, Yu H, Tong L, Chen D. Molecular signaling in temporomandibular joint osteoarthritis. J Orthop Translat. 2022;32:21–7. [CrossRef].
31. Cai S, Zou Y, Zhao Y, Lin H, Zheng D, Xu L, et al. Mechanical stress reduces secreted frizzled-related protein expression and promotes temporomandibular joint osteoarthritis *via* Wnt/β-catenin signaling. Bone. 2022;161:116445. [CrossRef].
32. Masuda T, Ishitani T. Context-dependent regulation of the β-catenin transcriptional complex supports diverse functions of Wnt/β-catenin signaling. J Biochem. 2017;161(1):9–17. [CrossRef].